Fabrication of $Fe_{16}N_2$ Films by Sputtering Process and Experimental Investigation of Origin of Giant Saturation Magnetization in $Fe_{16}N_2$

Jian-Ping Wang[1], Nian Ji[1], Xiaoqi Liu[1], Yunhao Xu[1], C. Sánchez-Hanke[2], Yiming Wu[1], F. M. F. de Groot[3], Lawrence F. Allard[4], and Edgar Lara-Curzio[4]

[1]Department of Electrical and Computer Engineering and the Center for Micromagnetics and Information Technologies (MINT), University of Minnesota, Minneapolis, MN 55455 USA

[2]National Synchrotron Light Source, Brookhaven National Laboratory, Upton, NY 11973 USA

[3]Inorganic Chemistry and Catalysis, Debye Institute for Nanomaterials Science, Utrecht University, 3584 CA Utrecht, The Netherlands

[4]High Temperature Materials Laboratory Microscopy Group, Materials Science and Technology Division, Oak Ridge National Laboratory, Oak Ridge, TN 37831 USA

We present a systematic study to address a longstanding mystery in magnetic materials and magnetism, whether there is giant saturation magnetization in $Fe_{16}N_2$ and why. Experimental results based on sputtered thin film samples are presented. The magnetism of $Fe_{16}N_2$ is discussed systematically from the aspects of material processing, magnetic characterization and theoretical investigation. It is observed that thin films with $Fe_{16}N_2$ + Fe_8N mixture phases and high degree of N ordering, exhibit a saturation magnetization up to 2.68T at room temperature, which substantially exceeds the ferromagnetism limit based on the traditional band magnetism understanding. From X-ray magnetic circular Dichorism (XMCD) experiment, transport measurement and first-principle calculation based on LDA+U method, it is both experimentally and theoretically justified that the origin of giant saturation magnetization is correlated with the formation of highly localized 3d electron states in this Fe-N system. A large magnetocrystalline anisotropy for such a material is also discussed. Our proposed "cluster+atom" theory provides promising directions on designing novel magnetic materials with unique performances.

***Index Terms*—FeN, $Fe_{16}N_2$, giant saturation magnetization, high magnetic moment, magnetic head, permanent magnet, XMCD, X-ray magnetic circular dichorism.**

I. Introduction

PURSUING magnetic materials with giant saturation magnetization (M_s) has huge impacts both scientifically and technologically. However, this effort has been fundamentally shadowed for decades by the famous Slater-Pauling curve [1], which is based on the classical itinerant magnetism theory. So far, the highest M_s value that can be predicted by first principles calculation is 2.45 T for $Fe_{65}Co_{35}$ alloy that has been used in magnetic writers [2].

About 40 years ago, Kim and Takahashi [3] first reported a material with a giant saturation magnetization that surpasses $Fe_{65}Co_{35}$ alloy, which was known as the material with highest saturation magnetization at the moment. 20 years later, Sugita's group [4] at Hitachi published a study that we saw as producing convincing evidence that the compound $Fe_{16}N_2$ exhibited giant saturation magnetization, and in particular a magnetic moment per Fe atom, well above any conventional theoretical prediction. That publication was followed by many others. Unfortunately, many of them were not able to reproduce the giant saturation magnetization results [5], and some claimed there is no giant saturation magnetization in this material [6], [7]. Investigators, including theoreticians, weighed in on one side of this question or the other. In particular, at the annual conference on Magnetism and Magnetic Materials in 1996, a symposium was held on the topic $Fe_{16}N_2$. Many of the researchers in this exciting field presented apparently conflicting views on the understanding of, perhaps, the most promising material for magnetic applications. The papers were published in [8]. No decisive conclusion was drawn on whether $Fe_{16}N_2$ has giant saturation magnetization at that time. Since then, this research topic has been dropped by most of magnetic researchers.

Wang's group at Minnesota has worked on this topic seriously since 2003. We realized that there have been four missing pieces (pillars) for this topic in past, which are interconnected with each other. First and most important, there is no convincing first-principles-based theory to support a giant M_s to go beyond FeCo. From the theoretical viewpoint, the local spin density approximation (LSDA)-based calculation yields an average magnetic moment no more than 2.5 μ_B per Fe [9]–[12] (M_s of 2.3T), but ambiguity remains since the Coulomb correlation energy of the 3d electrons is in general underestimated in the LSDA scheme. Secondly, there is lack of experiments using advanced probing techniques (e.g., synchrotron based X-ray) to explore its fundamental magnetism at a microscopic level, in which case, again, any convincing information extracted from this material system should rely on measurement on samples with high perfection or rigorous characterization. Thirdly, from the material viewpoint, it is extremely difficult to synthesize a pure phase $Fe_{16}N_2$ sample. Until now, only one group was able to fabricate single phase and single crystal thin films using Molecular Beam Epitaxy almost 20 years ago [4]. There is no easy-to-access thin film deposition process and recipe for academic research groups to repeatedly prepare $Fe_{16}N_2$ samples with controllable phase. Efforts have been focused on the "inferred" M_s of $Fe_{16}N_2$ phase based on the average M_s value measured from samples with a

Manuscript received August 02, 2011; accepted September 16, 2011. Date of current version April 25, 2012. Corresponding author: J.-P. Wang (e-mail: jpwang@umn.edu).

Color versions of one or more of the figures in this paper are available online at http://ieeexplore.ieee.org.

Digital Object Identifier 10.1109/TMAG.2011.2170156

mixture of different iron nitrides, in which case, the error bar caused by the determination of volume fraction and the estimation of M_s on other iron nitrides phases could easily overcome the $Fe_{16}N_2$ contribution. Fourthly, there is no clear physics and explanation behind the inconsistency for all the experimental reports. This further blocks new researchers from entering this field. Due to "these interconnected missing pieces," $Fe_{16}N_2$ remained a material mystery among magnetic researchers [13] until we recently reported our theoretical study on the origin of the giant saturation magnetization of $Fe_{16}N_2$ [14], [15].

In this paper, we present our systematic experimental effort on the $Fe_{16}N_2$ by collectively and successfully addressing the four missing pieces on this topic through our seven years' effort. Several findings that we considered as key building blocks to this research topic will be reported in details: 1) repeatable fabrication of partially ordered $Fe_{16}N_2$ samples with giant saturation magnetization by using a unique low-energy and plasma-free sputtering process; 2) discovery of the local 3d electron states in Fe_8N and $Fe_{16}N_2$ by using an element-specific magnetic characterization tool: synchrotron X-ray magnetic circular dichroism (XMCD); 3) finding of the N ordering effect on the magnetic behavior; 4) most importantly, developing a convincing theory to explain the origin of the giant saturation magnetization.

II. Experiment and Calculation

Epitaxial $Fe_{16}N_2$ thin films are fabricated by a facing target sputtering method. In this study, X-ray diffraction (XRD), X-ray reflectivity (XRR), transmission electron microscopy (TEM), and Auger Electron Spectroscopy (AES) experiments are conducted to determine the structural information of the prepared films. Vibrating sample magnetometry (VSM) is used to measure the in-plane M-H loops at room temperature. The temperature dependent transport properties are characterized Physical Property Measurement System (PPMS). To explore the localized feature and perform fundamental magnetism study, different Fe-N single phase samples are studied by x-ray absorption (XAS) and x-ray magnetic circular dichroism (XMCD) at National Synchrotron Light Source (NSLS), Brookhaven National Laboratory. A first principle calculation is performed using Vienna Ab-initial Simulation Package (VASP) code. In Section III, results based on these experiments and calculations are presented in an attempt to address the four "missing pieces" as stated previously.

III. Results and Discussion

A. Repeatable Fabrication of Partially Ordered $Fe_{16}N_2$ Samples With Giant Saturation Magnetization

1) Sample Fabrication: In this study, we have used facing target sputtering method. Fig. 1 shows the schematic diagram of the facing target sputtering system we used for this work. This system consists of two 4 inch circular Fe targets, placed face to face at a distance of ~10 cm. Two cylindrical permanent magnets are installed directly behind the water cooling cathodes, generating a magnetic field around 100 ~ 200 Oe with field direction perpendicular to the target surface. During the discharging process, electrons oscillate in the space between two targets in a helical motion due to the combined effects of both magnetic and electrical fields, which effectively improves the collision efficiency. More importantly, given this geometry, rather than charged ions, neutral atoms are more tentative to reach the substrate, which largely reduces the radiation damage of the plasma as well as the number of defects in the film during growth. This is of particular importance for the synthesis of such metastable phases and later on the post annealing process. Epitaxial Fe_8N+$Fe_{16}N_2$ samples were synthesized in the following method. GaAs (001) single crystal wafers were used as the substrate, and prior to the Fe-N growth, an Fe(001) underlayer was deposited to induce the Fe-N (001) texture at a substrate temperature of 250°C using pure argon as sputtering gas with a deposition rate of ~ 4.0 Å/s and a working pressure of ~4 mTorr. The iron nitrides layer is subsequently deposited by means of sputtering iron target with an appropriate mixture of Ar and N_2 with a total working pressure of 4 mTorr at room temperature. Fig. 2(a) shows the phase diagram obtained by tuning the N_2 partial pressure while fixing every other parameters (specified in the figure caption) during the deposition. The phase information are obtained from XRD. From the phase diagram, it is seen that by allowing the N_2 partial pressure to vary from 0 to 0.4 mTorr during deposition, c-lattice constant of Fe-N martensite is tunable in a wide range (Fig. 2(b)). Further increase of the N_2 pressure results in the formation of a nitrogen-rich Fe_4N phase. Refined tuning at the neighborhood of supersaturation threshold allows the optimization of Fe-N martensite with atomic ratio around 8/1 (checked by AES) with better crystal perfection. However, although the Fe-N martensite bct phase can be directly synthesized and shows good epitaxial adaption, we were unable to obtain the $Fe_{16}N_2$ phase from a direct deposition using the sputtering process, which requires N to interstitially occupy every other octahedral site in an orderly fashion. This is extremely difficult due to the thermodynamically more stable competing nitrogen rich phases (e. g. γ'-Fe_4N) during the sputtering process [16].

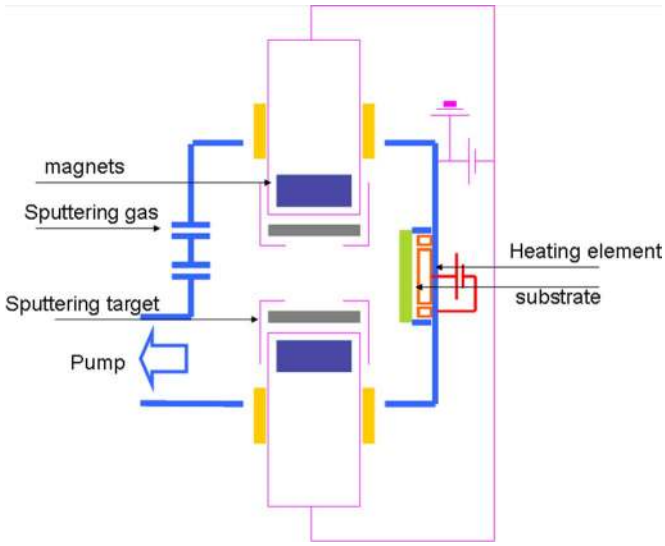

Fig. 1. Schematic of the facing target sputtering system and the location of targets, substrate, heater, working gas and pump.

After *in situ* post annealing samples at substrate temperature of 120°C, the diffraction peak at 28.6° develops, which can be

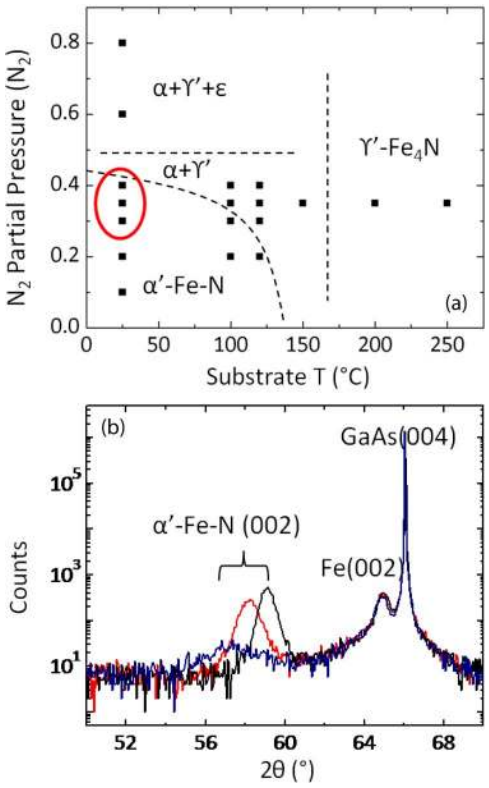

Fig. 2. (a) Fe-N phase diagram of thin films fabricated on Fe (001) buffered GaAs (001) substrate by FST. (b) Typical XRD spectrum of α'-Fe-N (Fe_8N) as it approaches the oversaturation limit in the martensite solid solution.

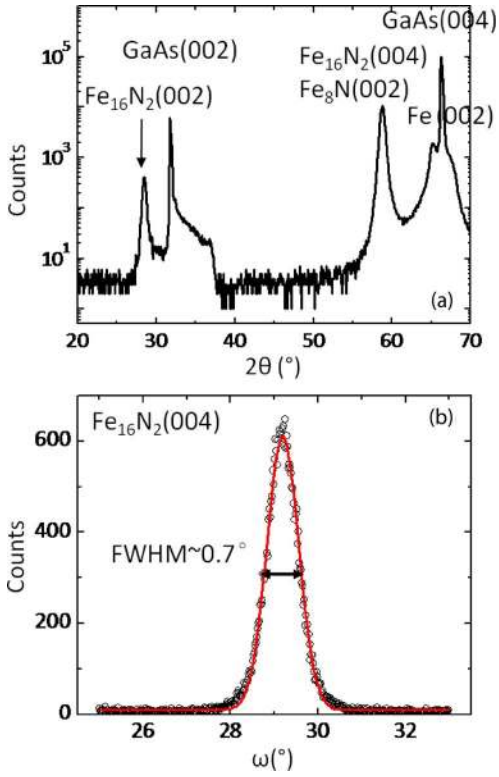

Fig. 3. (a) XRD on post-annealed $Fe_{16}N_2$ sample. (b) Rocking curve measured on $Fe_{16}N_2(004)$ with FWHM $\sim 0.7°$.

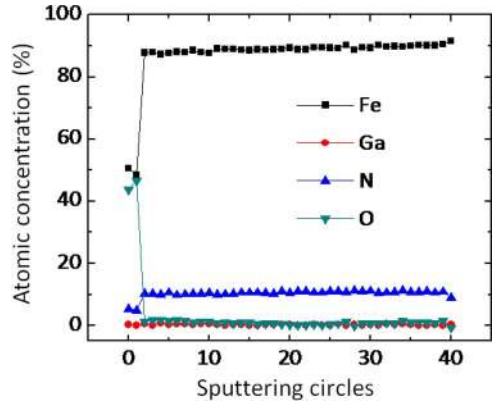

Fig. 4. Auger depth profile on post annealed $Fe_{16}N_2$ sample.

indexed as $Fe_{16}N_2(002)$. The corresponding d-spacing is doubled in comparison with Fe-N martensite (002). This suggests the appearance of long range chemically ordered N occupation. A typical XRD is shown in Fig. 3(a). The texture deviation as evaluated by Rocking Curve on the $Fe_{16}N_2(004)$ is shown with its full width of half maximum (FWHM) is determined to be $\sim 0.7°$ (Fig. 3(b)). In consistent with our previous report [17], the degree of N site ordering as defined by the integrated intensity ratio from the X-ray diffraction peaks $(I_{(002)}/I_{(004)})$ deviates from the structure factor calculation based on single crystal $Fe_{16}N_2$ and typically yields an ordering parameter 0.3 $\sim$ 0.35, which is defined as

$$D = \frac{I^{obs}(002)/I^{obs}(004)}{I^{cal}(002)/I^{cal}(004)}.$$

where $I^{obs}(002)$ and $I^{obs}(004)$ denote the integrated intensity of Bragg peaks of $Fe_{16}N_2(002)$ and (004) planes according to the XRD measurement. $I^{cal}(002)$ and $I^{cal}(004)$ represent integrated intensity these two peaks calculated from fully ordered $Fe_{16}N_2$.

2) Structural Characterization: The atomic concentration (Fe, N, O, C and Ga) of the partially ordered film with thickness around 100 nm is characterized by Auger depth profile as shown in Fig. 4. A uniform distribution of N and Fe inside the film with atomic ratio Fe/N $\sim 8/1$ is observed. A sharp drop of N at.% is observed at the Fe-N/Fe interface, suggesting no significant N diffusion occurs even annealing process is involved. It is important to notice that less than 1% O is detected in these films. Potential elements such as As, Ga, C can not be detected inside the films.

For thin film samples, it is known that one of the main sources of error bars on determining the M_s is the sample thickness measurement. To resolve this problem, two techniques are used to measure the same sample to ensure the accuracy. In Fig. 5(a), we show background subtracted XRR data of a prepared sample, which is fitted by a two layer model with the structural information outlined in the figure. The same sample is also prepared in cross-section TEM specimen. The image is shown in Fig. 5(b). The layered structure and the well-defined Fe-N/Fe interface are clearly visible given the microstructure and morphology contrast between these two layers. The corresponding

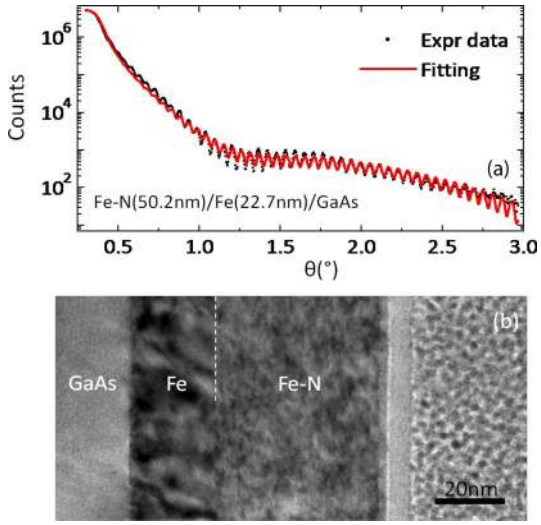

Fig. 5. (a) Typical XRR curve of Fe-N/Fe/GaAs sample with the fitted thickness structure shown in the figure. (b) Bright-field TEM cross-section image for the same sample; the layer structure is well-resolved by diffraction contrast.

thicknesses match reasonably well with that obtained from the XRR simulation.

3) Saturation Magnetization: The total magnetic moments were measured by using a vibrating sample magnetometer (VSM), which was calibrated by a standard Ni sample at room temperature. Samples are cut into squares approximately 5×5 mm in size. To precisely evaluate the film area, two methods were applied in order to minimize the error: 1) samples subject to VSM test were cut into a rectangular shape, and the total areas were calculated by measuring the side lengths using a micrometer; 2) the total mass of the same sample was measured and compared with the weight of a reference GaAs substrate with known area. The differences in the value of the sample area obtained between these two methods were treated as the error bar, which was $<2\%$. In order to subtract the diamagnetic contribution from the measured data and rule out possibility of any additional contribution from the magnetic impurities within the substrate, M-H loops from the pieces of substrate used for each film were subtracted from the corresponding raw data of the film. The absolute value of magnetization typically fell within the range of $10^{-3} \sim 10^{-4}$ emu, with testing error of $\sim$3%. First, to evaluate the magnetic contribution of the Fe seed layer, Fe/GaAs samples with different thickness were purposely grown to determine its saturation magnetization contribution as shown in Fig. 6. Subsequently, the magnetization of the Fe-N layer was calculated by subtracting the Fe seed layer contribution with the assumption of the M_s for the Fe seed layer to be 2.02 Tesla according to average value obtained here. Fig. 6 also plots the M_s of the pure Fe_8N samples with different film thicknesses, a typical M_s of 2.18 T is observed. It is worth noticing that the M_s evaluated from the prepared pure Fe samples is lower than that of its bulk value. This is likely due to the formation of Fe/GaAs interfacial phases, in which case, its magnetization is subtle to assess based on VSM approach. However, this is confirmed in our recent depth dependent polarized neutron reflectivity magnetic characterization study (not shown here).

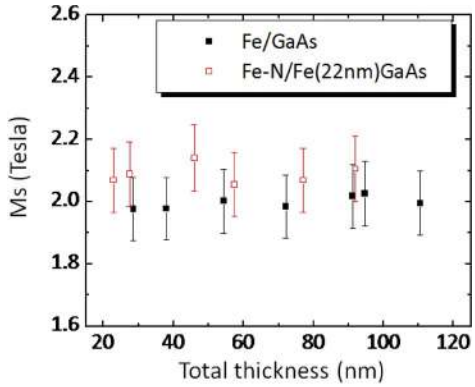

Fig. 6. Saturation magnetization on Fe and as-deposited Fe-N (Fe_8N) thin films as a function of film thickness. In the Fe-N samples, all the Fe underlayer is fixed to be 22 nm.

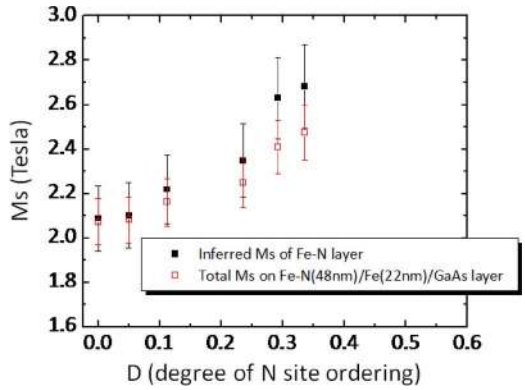

Fig. 7. Saturation magnetization as a function of D degree of N site ordering (see text) with a fixed layer structure as specified.

After annealing, samples with different ordering parameter D can be obtained. Fig. 7 shows the M_s measured in Fe-N/Fe/GaAs samples as a function of degree of N ordering (D). It is seen that as the D increases, the M_s of the whole film increases accordingly, arrives at a point of 2.47T at $D \sim 0.33$ and the calculated M_s for that Fe-N layer is $\sim$2.68 T. Therefore, saturation magnetization significantly exceeding the FeCo alloy is observed in films prepared here.

In addition to develop giant M_s, it is also clear that the Fe-N films develop crystalline anisotropy perpendicular to the thin film plane. Fig. 8 shows the hysteresis loops of partially ordered Fe-N/Fe/GaAs and Fe/GaAs samples. Besides the huge difference in the saturation magnetization, it is obvious that remanent magnetization (M_r) in the Fe film is almost equal to the saturation magnetization, indicating the easy axis is along the in-plane direction. On the other hand, with the presence of the Fe-N layer, the remanence (M_r) is much smaller than M_s. These results can be interpreted as that the easy axis of Fe-N/Fe/GaAs films exists out of thin film plane, which can be attributed to the perpendicular anisotropy due to the bct structure in Fe_8N and $Fe_{16}N_2$. In particular, as the applied field varies from zero to the saturation field (H_s), the magnetization of the film starts with a switching process due to domain movement, followed by a coherent rotation as the applied field goes beyond H_c. Thus, the perpendicular anisotropy is exclusively determined by H_s measured in plane and average M_s. Furthermore, plotted in Fig. 9(a) is H_s mea-

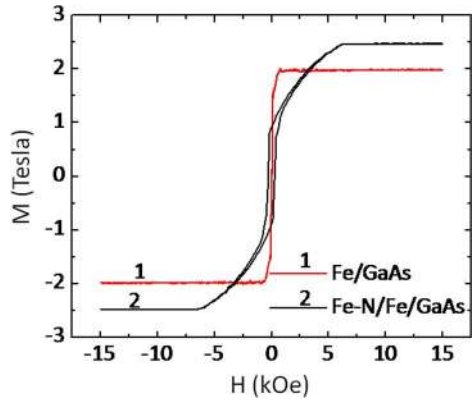

Fig. 8. M-H loops measured on Fe/GaAs and post annealed Fe-N/Fe/GaAs with thickness specified in text.

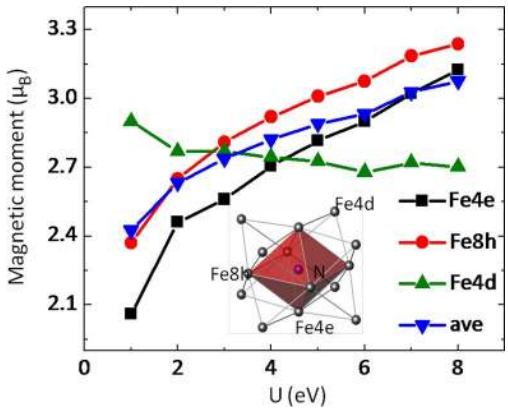

Fig. 10. Atom (Fe4d)+ cluster(Fe4e and Fe8h) model calculation: Local magnetic moment of three different Fe sites in $Fe_{16}N_2$ versus on site U.

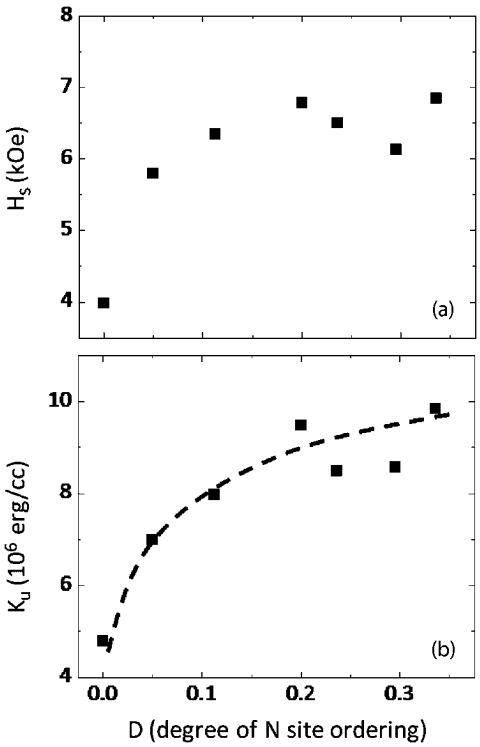

Fig. 9. (a) Saturation magnetization vs. N site ordering (D); (b) uniaxial anisotropy as a function of N site ordering.

sured on a series of Fe-N/Fe/GaAs with fixed thickness on each layer (Fe-N(48 nm)/Fe(22 nm)/GaAs) as a function of N ordering (D). It is seen that the H_s increases rapidly and saturates as D increases with a typical range from 4 $\sim$ 7 kOe. By applying the equation, the effective perpendicular anisotropy (K_u) of the Fe-N/Fe/GaAs films is plotted in Fig. 9(b), and the Ku of the Fe-N layer is estimated by assuming the K_p for the Fe seed layer is much smaller than that of the Fe-N layer. It is important to notice that the K_p as well as H_s obtained here closely resembles the perpendicular anisotropy measured by torque curve on the single phase high M_s samples. However, the shape anisotropy developed here is expected to be larger than K_u, in which case, the magnetization domain lies out of film surface but cannot reach the perpendicular direction to the sample surface.

B. Discovery of the Local 3d Electron States ATOM

1) Atoms (Fe) + Clusters (Fe_6N) Model: As governed by the Slater-Pauling Curve, it is known that itinerant ferromagnetism predicts the existing limit that the highest saturation magnetization for a material achievable so far is 2.45 T realized in $Fe_{65}Co_{35}$ alloy, which originates from the imbalanced occupation of the 3d spin up and down electron bands. Though ionic transition elements such as Fe^{3+} possess local magnetic moment up to 5 μB per iron atom, they usually exist in solids with ferrimagnetic or antiferromagnetic order and are always accompanied with large volume percentage of non-magnetic ions such as O^{2-} or S^{2-}, which significantly reduces the saturation magnetization (M_s). Therefore, to realize the giant saturation magnetization, one possible scenario is the coexistence of localized and itinerant electrons, the former provides the giant moment and the latter guarantees the ferromagnetic order.

In our previous study [14], an "atom + cluster" model was proposed to explain the giant saturation magnetization in $Fe_{16}N_2$. It was demonstrated that an unusual correlation effect arises within the Fe-N octahedral cluster region and the effective on-site 3d-3d Coulomb interaction increases due to a substantial 3d electrons charge density difference between interior and exterior clusters as schematically illustrated in Fig. 10, which leads to a partially localized electron configuration with a long range ferromagnetic order. First principle calculation based on LDA+U method [18] shows that giant saturation magnetization can be achieved at sufficiently large Hubbard U values. In particular, the U value of Fe outside (Fe4d) the cluster sphere was fixed at 1 eV and the magnetic moment change was then plotted for three Fe sites as the U inside the cluster (same U is assumed for both Fe4e and Fe8h) varied. The J parameter (Stoner parameter) was taken to be U/10. Calculations were performed by using the Vienna ab initio simulation package (VASP), with Projector Augmented Wave potential [19]. A plane wave cutoff corresponding to a kinetic energy of 250 eV was used. A k mesh of 8*8*8 was used to sample the supercell. The exchange correlation function was approximated with the fully localized limit of the local spin density approximation +U method [20]. The lattice constant was constrained according to its bulk value. The density of states (DOS) were calculated with fine k meshes using a tetrahedron method with Blöchl

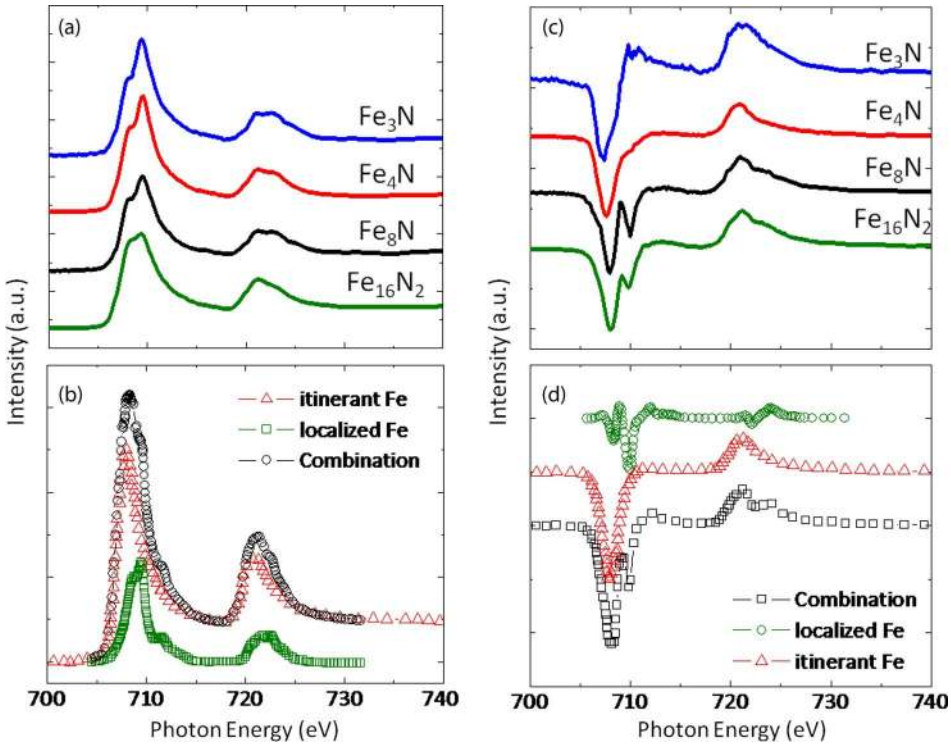

Fig. 11. (a) Fe L edge XAS for various Fe-N phase thin-film samples. (b) XAS simulation of localized and itinerant Fe L edge spectra. (c) Fe L edge XMCD measured on various Fe-N thin films. (d) XMCD simulation on localized and itinerant Fe L edge spectra.

corrections as implemented in VASP. Both Fe4e and Fe8h sites are sitting inside the Fe-N octahedral cluster. As the U increases, they favor rapid polarization while for the Fe4d site, which sits outside the Fe-N cluster, exhibits slow decay of the moment from 2.9 to 2.6 μB/Fe and levels off at high U values. It is seen that when U is large enough, an average magnetic moment above 3 μB/Fe is obtained. It is emphasized that the U is typically 1 $\sim$ 2 eV for metal Fe. However, in the present case, as the Fe-N forming the Fe6-N cluster, an unusual correlation can be brought up and consequently results in a strong enhancement of coulomb U.

2) XAS and XMCD Experiments: Encouraged by these results, X-ray magnetic circular dichroism (XMCD) experiments were carried out on a series of well textured Fe-N samples grown on single crystal (001) GaAs substrate. Plotted in Fig. 11(a) are the total-electron-yield mode iron L2,3 edges XMCD spectrum for single phase Fe_3N, Fe_4N, Fe_8N and partially ordered $Fe_{16}N_2$ samples, which were normalized to the L3 edge peak position. Similar to L edge XMCD data collected on pure iron metal, it is seen that the main excitation threshold occurs at the photon energy 708 $\pm$ 1 eV and 721 $\pm$ 1 eV for all these iron nitride samples, which is attributed to band-like states of the 3d electrons. Unexpectedly, it is obvious and interesting to notice, for the XMCD spectra of Fe_8N (α' phase) and partially ordered $Fe_{16}N_2$ (α'' phase) samples, there appear additional features on both edges. As shown in Fig. 11, this feature can be numerically reproduced by considering a spectrum of atomic-like Fe 3d6 to 2p53d7 multiplet transition in a D4h crystal symmetry superimposing with the band-like Fe, which provides solid evidence that two electron states (band-like and atomic like) coexist in Fe_8N and $Fe_{16}N_2$.

We also conclude that the ionic Fe contribution in the Fe_8N and Fe_8N_2 samples are not attributed to the presence of surface oxides. In the XAS data, it is seen that spectra for all these samples have metallic and ionic Fe signals due to surface native oxides. However, in the XMCD spectra, the ionic Fe signals are significantly reduced in Fe_3N and Fe_4N case and can be safely neglected. For the spectra of $Fe_{16}N_2$ and Fe_8N, the XMCD of the ionic signals are strong compared to the Fe_3N and Fe_4N cases.

3) Resistivity Measurement: Fig. 12 shows the resistivity versus temperature curve measured from 5 K to 300 K for partially ordered $Fe_{16}N_2$/Fe/GaAs and Fe/GaAs samples prepared here. Coincident with the observation by Sugita on their MBE samples, a giant residual resistivity is also present, which is significantly larger than metal Fe. Given that their samples are single-crystal, it is highly likely that such a constant resistivity background originates from the intrinsic properties of the $Fe_{16}N_2$ phase rather than from scattering by defects. The independent temperature resistivity behavior at low temperature was reported in thin films of the LaSrMnO system [21], which was attributed to the presence of phonon-less electrons tunneling, hinting at the existence of "atomic-like" electron states.

IV. N Site Ordering Effect

Now we discuss the conflicting observations of the M_s in this material system. In general, it is accepted that the ferromagnetism of 3d transition metals and their alloys is governed by the famous Slater-Pauling curve. In that case, a magnetic moment of 2.5 μB per atom is considered as the limit and realized in the $Fe_{0.65}Co_{0.35}$ alloy system at room temperature. This

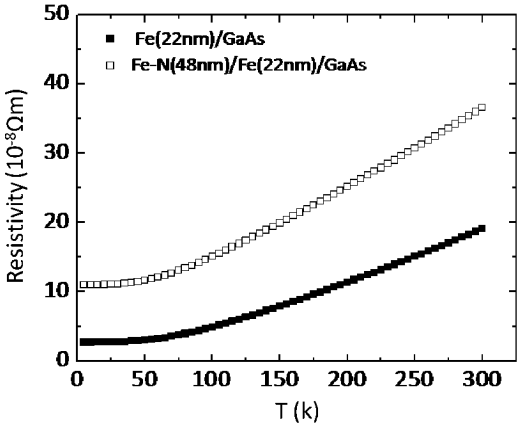

Fig. 12. Resistivity vs. Temperature curve for Fe on GaAs and partially ordered $Fe_{16}N_2$ on GaAs with Fe seed layer.

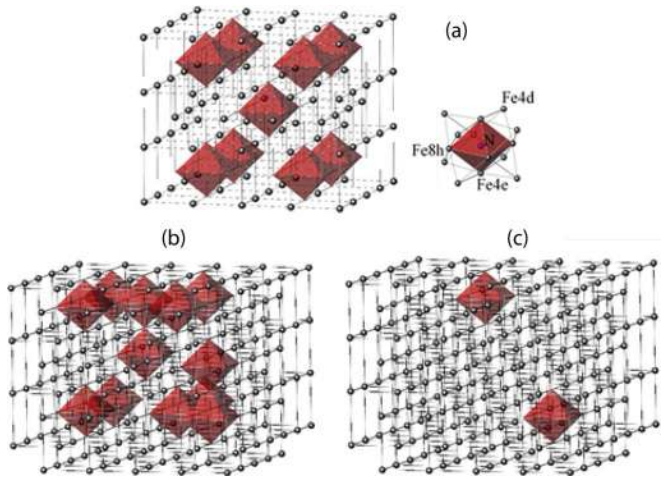

Fig. 13. (a) $Fe_{16}N_2$ crystal structure; (b) N rich local region in Fe_8N; (c) N poor local region in Fe_8N

is far below the experimental claim (3.2 μB/Fe) observed in the single-phase $Fe_{16}N_2$ samples ([4]), and in the sputtering-beam-prepared epitaxial samples (2.9 μB/Fe) [22] as well as in the present results (2.93 μB/Fe). It is also appealing to notice that in all these three experiments, the degree of N site ordering strongly affects the average magnetic moment of the Fe/N $= 8/1$ ($\alpha' + \alpha''$) system. In accordance with the proposed model (atom+cluster model), since the N atoms are arranged in an ordered fashion and occupy every other octahedral site, the key to realizing high moment is to establish "spatial isolation" of Fe-N clusters in the sense that no neighboring clusters are shared by a common iron atom site (Fig. 13(a)). In this case, strong Coulomb interaction arises due to the charge difference both interior and exterior to the cluster region, and consequently leads to the appearance of localized electrons on Fe sites within the Fe-N clusters (Fe4e and Fe8h), and itinerant band-like electrons on the rest of the Fe sites (Fe4d) outside the clusters. In the atomic limit, a magnetic moment of 4 μB/Fe is realized given Hund's first rule for highly localized electrons, and ~ 2.0 μB/Fe is considered for band-like electrons according to itinerant Fe. This will produce an average magnetic moment of ~ 3.5 μB/Fe for the chemically ordered $Fe_{16}N_2$. However, in the disordered Fe_8N, due to the N random occupation, there exists both N-rich and N-poor local regions, as schematically shown in Fig. 13(b) and (c). In the N-rich case, the Fe-N clusters are inevitably "connected" through their neighboring Fe-N clusters, in which the corner-shared or edge-shared Fe atoms are present. These Fe atoms closely resemble the local chemical environment of Fe sites in N-rich phases such as Fe_4N or Fe_3N. Consequently, the significant charge difference brought up in a "separated cluster" scenario disappears. Therefore, electrons residing on these sites evolve from highly localized atomic-like states to itinerant band-like states, again due to the reduction of Coulomb interaction. In the N-poor case, though the "cluster separation" is still maintained, the dominant population of Fe sites is metallic-like, which also leads to the reduction of average magnetic moment. To give a quantitative estimation, in α''-$Fe_{16}N_2$, 75% of iron sites (Fe4e and Fe8h) have only one N as the nearest neighbor (NN). The remaining 25% consists only of Fe4d with no surrounding N. However, in α'-Fe_8N, the percentage of iron sites with 0, 1, 2 and 3 N atom(s) as NN was

TABLE I

m	0	1	2	3	Total
P_m(%)	44.88	38.47	13.74	2.61	0.997

calculated under the binomial distribution assumption using the following equation. The result is summarized below

$$P_m = \frac{6!}{(6-m)!m!}\left(\frac{1}{8}\right)^m\left(1-\frac{1}{8}\right)^{n-m}$$

where P_m is defined as the percentage of the iron sites that have m N atoms as NN. Similarly, we consider that highly localized Fe sites ($\mathrm{m} = 1$ case) possess a magnetic moment of 4 μB and band-like Fe sites ($\mathrm{m} = 0, 2$ and 3) possess a moment of 2 μB. The average magnetic moment of 2.6 μB/Fe is obtained, which is substantially lower than that of $Fe_{16}N_2$. As for the N partially ordered case, a non-trivial scenario could occur if Fe-N clusters are interconnected in a macro scale, say a few hundreds of atoms, then the assumption of the magnetic moment of 4 μB/atom for the $\mathrm{m} = 1$ case would be no longer valid. From the perspective of bond percolation theory, the threshold impurity concentration Pc is 0.12 for an fcc lattice [23], which is less than that in Fe/N $= 8/1$ case ($\mathrm{p} = 0.125$). This suggests a random distribution of the N in this lattice system would cause a global connection of Fe-N octahedral clusters and give rise to band-like iron behavior. From a broader perspective, to rationalize the giant magnetic moment, it is essential to consider the formation of localized electron states where Hund's rule can be suitably applied. The present "cluster+atom" model considers the electron localization and explicitly discusses the evolution from localized to itinerant electron states of Fe due to the local chemical environment change, in which the N site ordering effect can be interpreted.

V. Conclusion

In summary, we present a systematic effort on the Fe by collectively and successfully addressing the four "missing pieces" of this topic. Several findings that we considered as key building

blocks to this research topic are reported in detail: 1) repeatable fabrication of partially ordered Fe samples with giant saturation magnetization by using a unique low-energy and plasma-free sputtering process; 2) discovery of the local 3d electron states in $Fe_{16}N_2$ by using an element-specific magnetic characterization tool: synchrotron X-ray magnetic circular dichroism (XMCD); 3) finding of the role of Fe6-N octahedral clusters; and 4) finding of the N ordering effect on the magnetic behavior.

VI. Outlook

We recently addressed the challenge for the direct measurement of the magnetic moment of Fe atoms, e.g., using the polarized neutron reflectivity method, and found direct evidence of charge transfer in the $Fe_{16}N_2$ system using the polarization-dependent x-ray absorption near edge spectroscopy (XANES) method. These results will be reported in another paper [24].

There are still several fundamental questions remaining unaddressed. In particular, 1) the unusual Mossbauer spectra performed on high Ms samples; 2) the first principles calculation based on LDA+U method requires a large U to obtain the giant Ms; The specific calculation of the U in $Fe_{16}N_2$ system hasn't been done yet;

Practically speaking, to fabricate pure $Fe_{16}N_2$ samples, challenges such as the preparation temperature, thermal instability (phase change between Fe_8N and $Fe_{16}N_2$) as well as the relatively large perpendicular anisotropy are remaining issues for real magnetic writer application or for rare-earth free permanent magnet application. Possible solutions are to introduce the underlayer epitaxial constraint and composition optimization to improve the thermal stability. Our proposed "cluster+atom" model provides promising directions on designing novel magnetic materials with unique performances. We believe there could be other material systems to go beyond $Fe_{16}N_2$ system.

Acknowledgment

The work was supported in part by the U.S. Department of Energy, Office of Basic Energy Sciences under contract No. DE-AC02-98CH10886, characterization facility of National Science Foundation the Minnesota MRSEC program under Award Number DMR-0819885, NSF NNIN program and University of Minnesota Supercomputing Institute. All the samples and testing experiments reported in this paper have been done before September 2009 (first report of our work at UMN MINT review 2009) based on above-mentioned financial support. The microscopy at HTML/ORNL was sponsored by U.S. DOE, Office of Energy Efficiency and Renewable Energy, Vehicle Technologies Program. The authors are grateful to the useful discussion with Drs. Valeria Lauter, Chengjun Sun, Hailemariam Ambaye, and Steve M Heald from DOE national labs (ORNL, ANL) and Profs. Jack Judy, Paul Crowell, and Randall Victora from the University of Minnesota.

References

[1] J. C. Slater, "Electronic structure of alloys," *J. Appl. Phys.*, vol. 8, pp. 385–390, 1937.

[2] R. C. O'Handley, *Modern Magnetic Materials Principles and Applications*. New York: Wiley, 2000.

[3] T. K. Kim and M. Takahashi, "New magnetic material having ultrahigh magnetic moment," *Appl. Phys. Lett.*, vol. 20, pp. 492–494, Dec. 1972.

[4] Y. Sugita, H. Takahashi, M. Komuro, K. Mitsuoka, and A. Sakuma, "Magnetic and Mössbauer studies of single-crystal $Fe_{16}N_2$ and Fe-N martensite films epitaxially grown by molecular beam epitaxy (invited)," *J. Appl. Phys.*, vol. 76, pp. 6637–6641, Nov. 1994.

[5] R. M. Metzger, X. H. Bao, and M. Carbucicchio, "Magnetism of α''-$Fe_{16}N_2$ (invited)," *J. Appl. Phys.*, vol. 76, no. 10, pp. 6626–6631, Nov. 1994, and references therein.

[6] M. Takahashi *et al.*, "Magnetic moment of α''-$Fe_{16}N_2$ films (invited)," *J. Appl. Phys.*, vol. 76, pp. 6642–6647, Nov. 1994.

[7] J. M. D. Coey, "The magnetization of bulk $\alpha''Fe_{16}N_2$ (invited)," *J. Appl. Phys.*, vol. 76, pp. 6632–6636, Nov. 1996.

[8] *J. Appl. Phys.*, vol. 79, pp. 5564–5581, Nov. 1996, Symposium on $Fe_{16}N_2$ (chairperson: T. Suzuki) and all references therein.

[9] M.-Z. Huang and W. Y. Ching, "Spin-density distribution in ferromagnetic α''-$Fe_{16}N_2$," *Phys. Rev. B*, vol. 51, no. 5, pp. 3222–3225, Feb. 1995.

[10] H. Tanaka, H. Harima, T. Yamamoto, H. Katayama-Yoshida, Y. Nakata, and Y. Hirotsu, "Electronic band structure and magnetism of $Fe_{16}N_2$ calculated by the FLAPW method," *Phys.Rev. B*, vol. 62, no. 22, pp. 15042–15046, Dec. 2000.

[11] G. W. Fernando, R. E. Watson, M. Weinert, A. N. Kocharian, A. Ratnaweera, and K. Tennakone, "Magnetic moment of iron in metallic environments," *Phys. Rev. B*, vol. 61, no. 1, pp. 375–381, Jan. 2000.

[12] A. Sakuma, "Electronic and magnetic structure of iron nitride, $Fe_{16}N_2$ (invited)," *J. Appl. Phys.*, vol. 79, no. 8, pp. 5570–5575, Nov. 1996.

[13] J. P. Wang, in *INSIC Meeting 2010; APS Meeting 2010; ScienceNOW*, Mar. 19, 2010.

[14] N. Ji, X. Q. Liu, and J.-P. Wang, "Theory of giant saturation magnetization in α''-$Fe_{16}N_2$: Role of partial localization in ferromagnetism of 3d transition metals," *New J. Phys.*, vol. 12, no. 6, pp. 063032–063039, Jun. 2010.

[15] X. Q. Liu, Y. H. Xu, C. Hanke, and J.-P. Wang, "Discovery of Localized States of Fe 3d Electrons in $Fe_{16}N_2$ and Fe_8N Films: An Evidence of the Existence of Giant Saturation Magnetization," arxiv: 0909.4478.

[16] D. C. Sun, E. Y. Jiang, M. B. Tian, C. Lin, and X. X. Zhang, "Epitaxial single crystal $Fe_{16}N_2$ films grown by facing targets sputtering," *J. Appl. Phys.*, vol. 79, pp. 5440–5442, Apr. 1996.

[17] N. Ji, L. F. Allard, E. Lara-Curzio, and J.-P. Wang, "N site ordering effect on partially ordered $Fe_{16}N_2$," *Appl. Phys. Lett.*, vol. 98, pp. 092506–092508, Jan. 2011.

[18] V. I. Anisimov, J. Zaanen, and O. K. Anderson, "Band theory and Mott insulators: Hubbard U instead of Stoner I," *Phys. Rev. B*, vol. 44, pp. 943–954, Jul. 1991.

[19] P. E. Blöchl, "Projector augmented-wave method," *Phys. Rev. B*, vol. 50, pp. 17953–17979, Dec. 1994.

[20] V. Anisimov, F. Aryasetiawan, and A. Lichtenstein, "First principles calculations of the electronic structure and spectra of strongly correlated systems: The LDA+ U method," *J. Phys. Condens. Matter.*, vol. 9, pp. 767–808, Jul. 1996.

[21] V. D. Okunev, N. N. Pafomov, A. Abaleshev, H. Belska-Lewandowska, P. Gierlowski, AKlimov, and S. Lewandowski, "The low-temperature electric conductivity of YBaCuO and LaSrMnO dielectric films obtained by a pulsed laser sputter deposition technique," *Tech. Phys. Lett.*, vol. 26, pp. 903–906, Oct. 2000.

[22] S. Okamoto, O. Kitakami, and Y. Shimada, " α''-$Fe_{16}N_2$ phase epitaxially grown by sputter beam method," *J. Appl. Phys.*, vol. 79, no. 8, pp. 5250–5252, Nov. 1996.

[23] C. D. Lorenz and R. M. Ziff, "Precise determination of the bond percolation thresholds and finite-size scaling corrections for the sc, fcc, and bcc lattices," *Phys. Rev. E*, vol. 57, pp. 230–236, Jan. 1998, for a bct structured $Fe - N'$, the crystal structure viewed along 110 direction closely resembles the fcc lattce matrix.

[24] N. Ji, V. Lauter, C. J. Sun, H. Ambaye, S. M. Heald, X. Q. Liu, Y. H. Xu, X. Li, and J. P. Wang, "Direct observation of giant saturation magnetization in $Fe_{16}N_2$ by polarized neutrons reflectivity and X-ray absorption near-edge spectroscopy," to be published.